Research Article Vol. 62, No. 19 / 1 July 2023 / Applied Optics 5301

applied optics

Remote sensing oil in water with an all-fiber underwater single-photon Raman lidar

Mingjia Shangguan,[1,*] Zhifeng Yang,[1] Mingyu Shangguan,[2] Zaifa Lin,[1] Zhuoyang Liao,[1] Yirui Guo,[1] and Chuan Liu[3]

[1]State Key Laboratory of Marine Environmental Science, College of Ocean and Earth Sciences, Xiamen University, Xiamen 361102, China
[2]Fuzhou Dayu Electronic Technology Co., Ltd., Fujian 350021, China
[3]Innovation Laboratory for Sciences and Technologies of Energy Materials of Fujian Province (IKKEM), Xiamen 361005, China
*mingjia@xmu.edu.cn

Received 6 March 2023; revised 25 May 2023; accepted 29 May 2023; posted 30 May 2023; published 29 June 2023

The detection of oil in water is of great importance for maintaining subsurface infrastructures such as oil pipelines. As a potential technology for oceanic application, an oceanic lidar has proved its advantages for remote sensing of optical properties and subsea materials. However, current oceanic lidar systems are highly power-consuming and bulky, making them difficult to deploy underwater to monitor oil in water. To address this issue, we have developed a compact single-photon Raman lidar by using a single-photon detector with high quantum efficiency and low dark noise. Due to the single-photon sensitivity, the detection of the relatively weak Raman backscattered signal from underwater oil was realized with a laser with a pulse energy of 1 μJ and a telescope with a diameter of 22.4 mm. An experimental demonstration was conducted to obtain the distance-resolved Raman backscatter of underwater oil of different thicknesses up to a distance of 12 m. The results indicate the single-photon Raman lidar's potential for inspecting underwater oil pipelines.

https://doi.org/10.1364/AO.488872

1. INTRODUCTION

The detection of oil in seawater is of paramount importance for ocean observation and exploration, as well as for the maintenance of subsea infrastructures, such as pipeline inspection [1,2]. The early detection of oil spills is also essential to minimize their environmental and economic impacts. Oil spills can cause significant damage to both freshwater and marine ecosystems, including physical harm to wildlife and their habitats [3].

The detection of oil, particularly in water, remains a significant challenge due to the complexity of the oceanic environment. To address this, researchers have developed various methods. One emerging solution for subsea inspection tasks is underwater robotics equipped with multiple sensors [4]. Raman spectroscopy, a conventional optical sensing methodology, has been widely utilized in underwater robotics due to its ability to detect multiple species simultaneously. This technology has been extensively employed for the detection of elements in extreme zones, such as hydrothermal vents and gas hydrate areas [5,6]. However, these point-sensing methods can be labor-intensive and expensive, presenting challenges when attempting to monitor long-distance pipelines and their associated infrastructures.

One of the most promising technologies for remote sensing of oil spills is the lidar, which has been extensively used for monitoring inherent optical properties of the atmosphere, water, soil, and forests [7–9]. Two kinds of lidar are currently used to remotely sense oil in the ocean, namely, the laser-induced fluorescence lidar and Raman lidar. Over the years, fluorescence lidars have shown great potential for detecting and discriminating oil and chemical pollutants spilled or dissolved in the sea [10,11], as well as phytoplankton [12] and algae species [13]. However, this approach is ineffective in identifying substances that cause similar light-induced fluorescence signals. In contrast, Raman spectroscopy offers high discrimination capabilities and can identify different materials, including oil and dissolved CO_2 in water [14]. However, due to the small cross section of Raman scattering, which is two to three orders of magnitude lower than the elastic scattering cross section, a laser with high pulse energy and a large-aperture telescope are required to improve the signal-to-noise ratio. This leads to a bulky and high power-consuming property of a Raman lidar, limiting its deployment underwater [15]. To address this issue, for the first time, to the best of our knowledge, we propose and demonstrate an underwater Raman lidar. This system allows for more efficient remote detection of oil leakage in water. Due to the limited water penetration distance of oceanic the lidar, deploying a lidar underwater will greatly extend its detection coverage and depth, with the assistance of underwater platforms, such as autonomous underwater vehicles (AUVs). AUVs will facilitate the inspection of underwater infrastructures, such as oil pipelines in a significant way.

To achieve oil stand-off detection with a low pulse energy laser and a small-aperture telescope, a single-photon detector is necessary due to the low Raman scattering cross section. By increasing the sensitivity of the atmospheric aerosol lidar detection to the single-photon level, we have demonstrated the long-range detection of atmospheric aerosols using microjoule pulsed lasers and centimeter-sized telescopes [16–18]. In contrast to our atmospheric lidars that operate at 1.5 μm wavelength, oceanic lidars usually work in the visible light band. This allows the use of commercially available and mature single-photon detectors, such as photomultiplier tubes (PMTs) and silicon avalanche photodiodes (Si-APDs). While both PMTs and Si-APDs can detect single photons in the visible band, we opted for Si-APDs due to their lower environmental requirements. Specifically, Si-APDs do not require a high-voltage power supply and are less susceptible to magnetic interference compared to PMTs [19].

The article is organized as follows. First, the Raman lidar system used for oil stand-off detection is introduced. Next, the preliminary results obtained using this system are presented. Finally, a conclusion is provided.

2. RAMAN LIDAR SYSTEM

To achieve high spatial resolution detection, we employed a picosecond pulsed laser and a high precision time-digital-converter (TDC). The results presented in this article demonstrate the feasibility of single-photon underwater Raman detection with a detection range of up to 12 m and an accumulation time of 5 s.

A schematic diagram of the single-photon Raman lidar system setup is illustrated in Fig. 1. The lidar consists of four subsystems, including a 532 nm laser, a transceiver, an optical receiver, and a data acquisition component. The system employs a compact fiber-based laser that is constructed following a master oscillator power amplifier architecture. The pulsed 1064 nm laser with a repetition rate of 1 MHz serves as a seed laser, and its output power is amplified by a three-stage amplifier, including a single-mode ytterbium-doped fiber amplifier (SM-YDFA) and a subsequent two-stage multimode high-power ytterbium-doped fiber amplifier (HP-YDFA). After amplification, frequency doubling from 1064 to 532 nm is carried out by using a lithium borate (LBO) crystal. This results in a pure green light with a pulse width of 501 ps and a pulse energy of 1 μJ. The laser has a beam divergence of 0.5 mrad.

A fiber-connected configuration is specially designed for miniaturization and a robust structure. The backscattered signal from water is coupled into a 105 μm multimode fiber (MMF) by an achromatic collimator with a focal length of 50.8 mm, which corresponds to a lidar field of view (FOV) of 2.1 mrad. This narrow receiver FOV provides a significant backscatter noise suppression. The distance between the transmitting laser and the receiving coupler is ~10 mm. The backscattered signal is then collimated by a lens. Behind the collimator lens, a 45° dichroic mirror and a notch filter ($Filter_1$) at 532 nm are placed to reflect the elastic signals caused by elastic scattering. A 628 nm filter ($Filter_2$) with a bandwidth of 5.5 nm is used to pick up the Raman signal and further block the background noise. It is worth noting that this article only verifies the feasibility of the single-photon underwater Raman lidar for underwater oil detection and, therefore, only uses a single-wavelength channel. Differentiating between different types of oil and even different substances in water requires more spectral channels with high spectral resolution (even at the picometer level) [5].

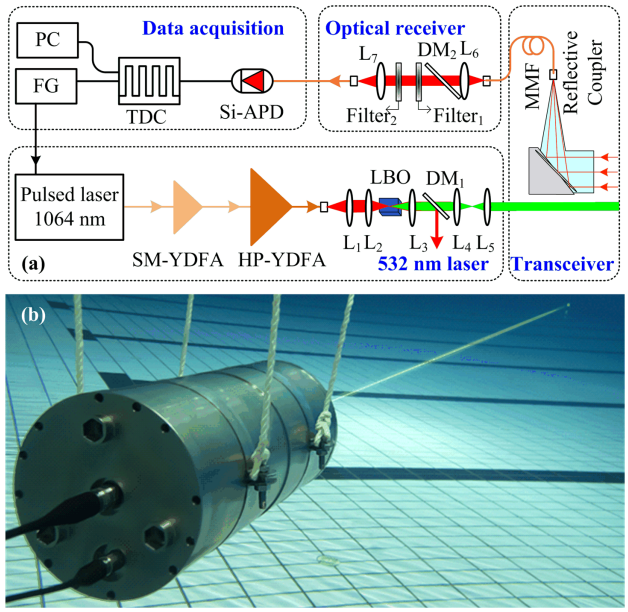

Fig. 1. (a) Schematic setup of the single-photon Raman lidar. SM-YDFA, single-mode ytterbium-doped fiber amplifier; HP-YDFA, high-power ytterbium-doped fiber amplifier; L, lens; LBO, lithium borate; MMF, multimode fiber; DM, dichroic mirror; Si-APD, silicon avalanche photodiode; TDC, time-digital-converter; FG, function generator; PC, personal computer. (b) Photograph of the underwater single-photon Raman lidar system.

Finally, the Raman lidar system incorporates a compact free-running Si-APD that continuously detects photons using its own internal clock without requiring any external clock or trigger signal synchronization. It has an efficiency of ~ 68 % with 100 dark counts per second (cps) at 628 nm.

As shown in Fig. 2, Raman spectra of oil and pure water were recorded by using a confocal Raman microscope (XploRA Horiba J.Y.) with a 532 nm laser. The oil used in the experiment was gasoline oil. The laser beam was focused by a 50 × /0.5NA objective lens. The laser power at the sample location was 15 mW. The exposition time was 5 s. The Raman spectrum of the oil shows a large spectral background, which is attributed to the fluorescence spectrum of the oil. As for the Raman spectrum of water, as shown in Fig. 2, the center position of its Raman line is around 650 nm, which is about 22 nm away from the center of the Raman line of oil located around 628 nm. The Raman band of 2900 cm^{-1} (corresponding to the wavelength of 628 nm) is generated by the stretching vibration of the C-H bond of the oil molecule.

As to the electronic module, a homemade function generator (FG) based on a field programmable gate Array provides a precise control signal for the laser and TDC. A high-precision TDC (Swabian Instruments, Time Tagger Ultra) with 13 ps resolution is adopted to record the time of the pulse emission and photon detection. The time jitter of the whole system was

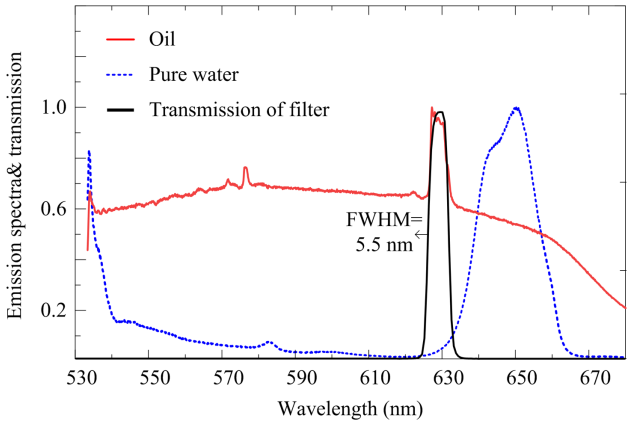

Fig. 2. Emission spectra of oil (red solid line) and pure water (blue dashed line) under 532 nm laser excitation, along with the transmission curve of the 628 nm filter (black solid line).

Table 1. Key Parameters of the Single-Photon Underwater Raman Lidar

Parameter	Value
Laser wavelength	532 nm
Pulse duration	501 ps
Pulse energy	1 μJ
Pulse repetition rate	1 MHz
Beam divergence	0.5 mrad
Diameter of telescope	22.4 mm
Focal length of coupler	50.8 mm
Mode-field diameter of MMF	105 μm
FOV of coupler	2.1 mrad
Bandwidth of the Raman filter ($filter_2$)	5.5 nm
Detection efficiency of the Si-APD at 628	68 %
Dark count of the Si-APD	100 cps
Size of the Raman lidar	φ20 cm × 40 cm
Power consumption of the Raman lidar	≤ 100 W

measured to be ∼1800 ps. A summary of the system parameters is listed in Table 1.

Due to its compactness and low power consumption, the lidar can be flexibly integrated into different platforms, such as an underwater platform described in this paper. A photograph of the underwater lidar system is shown in Fig. 1(b). The lidar system is made of a titanium alloy with high-pressure resistance properties so that the lidar can operate underwater for down to 1 km depth. The optical window of the lidar is made of a sapphire lens, which can maintain ≥ 96 % transmission under high pressure. The cylindrical lidar has a diameter of 20 cm and a length of 40 cm. The average power consumption of the lidar is less than 100 W.

3. PRELIMINARY EXPERIMENTS

Here a field experiment was carried out to demonstrate the performance of the single-photon Raman lidar for underwater oil detection in a swimming pool at the Xiang'an campus of Xiamen University (2437′N, 11818′E). The size of the pool is 50 × 25 × 2 m^3. In the experiment, the Raman lidar and a quartz cell filled with oil (gasoline) were submerged in water, with the quartz cell positioned 12 m away from the laser in its path. The Raman lidar and the quartz cell were fixed using aluminum frames and placed 0.6 m underwater. During the experiment, the circulating water system of the swimming pool was turned off to minimize the influence of surface ripples on the experimental results. The raw lidar profile with 5 s accumulation time and 5.6 cm spatial resolution is plotted in Fig. 3(a). An accumulation time of 5 s corresponds to a total of 5 million laser pulses emitted. In the near range from the lidar, the intensity of the backscattered signal (water Raman) first increases as the laser beam and the received FOV tends to overlap. Then the signal intensity decreases with the distance, but the water signal can be observed up to nearly 18 m. This capability of the lidar system is remarkable, since only the weak (micropulse) laser source is employed, and the water Raman signal is strongly suppressed due to the narrow bandpass filter centered at 628 nm (Fig. 2). In the experiment, oil thicknesses were measured at intervals of 1 mm, ranging from 1 to 15 mm. Figure 3(b) shows an example of an oil Raman signal obtained with a thickness of 8 mm, indicating that the peak of the profile at ∼12 m is due to the Raman backscattering of oil. The backscattered signal beyond 12 m in Fig. 3(b) exhibits a tail with a 1/e width of approximately 3 ns, which is attributed to several factors, including the pulsed laser width (0.5 ns), acquisition card jitter (13 ps), and detector time jitter (approximately 1.5 ns). Additionally, a small portion of the fluorescence signal from the oil passes through the Raman filter and is detected, contributing to the tailing of the backscattered signal. Studies have shown that the fluorescence lifetime from oil can range from several to tens of nanoseconds [20,21]. To mitigate interference from the fluorescence signal, we will use a shorter wavelength for the excitation laser and optimize the Raman filter bandwidth in our future work.

To analyze the relationship between the backscattered signal from the oil and its thickness, we fitted the oil's backscattered signal using the exponentially modified Gaussian function [22]:

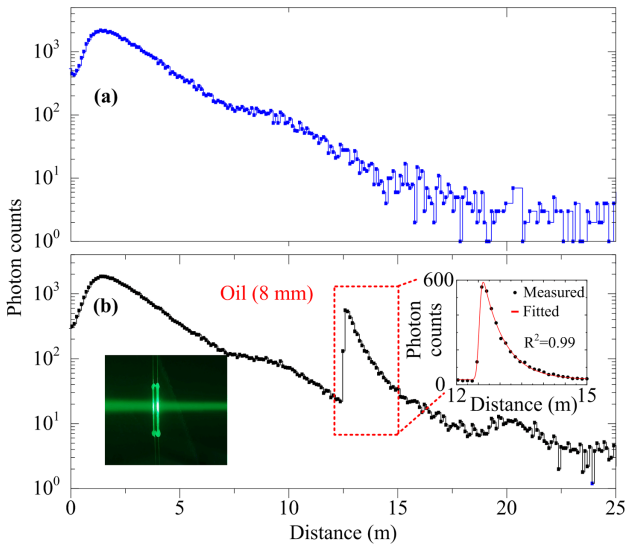

Fig. 3. (a) Backscattering Raman profile without oil and (b) backscattering Raman profile with oil (gasoline) located 12 m away from the lidar.

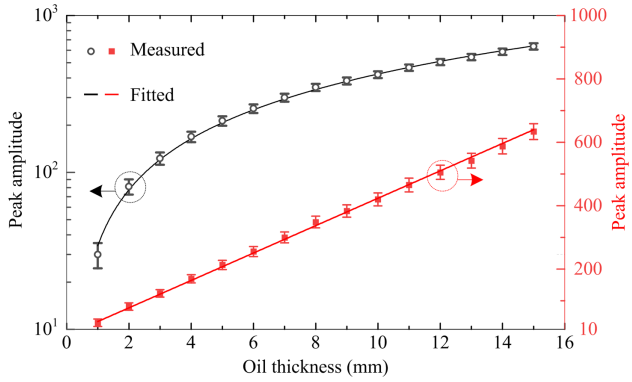

Fig. 4. Relationship between the Raman peak area of oil and oil thickness.

$$f(x) = y_0 + \frac{A}{t_0}\exp\left[0.5(w/t_0)^2 - (x - x_c)/t_0\right] \times \int_{-\infty}^{[(x-x_c)/w - w/t_0]} \frac{1}{\sqrt{2\pi}}\exp(-y^2/2)\mathrm{d}y, \quad (1)$$

where y_0 is the offset, A is the peak amplitude, t_0 is the time constant of the exponential decay function, w is the variance of the Gaussian, and x_c is the center of gravity of the Gaussian. For example, Fig. 3(b) shows the Raman backscattered signal with an oil thickness of 8 mm, while Fig. 3(a) shows the Raman backscattered signal without oil, which serves as a reference. Fitting the backscattered signal from 12 to 15 m to Eq. (1) yields the result shown in the inset of Fig. 3(b), with a fitted R-Square value of 0.99.

Subsequently, the relationship between the fitted peak amplitude (A) and oil thickness was analyzed quantitatively by measuring the backscattered signals at different oil thicknesses and using Eq. (1) for fitting. As shown in Fig. 4, a good linear relationship between the fitted peak amplitude (A) and oil thickness was obtained, which is consistent with the results of previous studies [15]. To better display the measurement results, we present Fig. 4 with dual axes, i.e., logarithmic and linear scales. The linear regression analysis between the fitted peak amplitude (A) and oil thickness yielded an R-square of up to 0.99. To verify the measurement stability, we conducted 10 sets of measurements at each oil thickness. Figure 4 displays the variances of the fitted peak amplitudes obtained at different oil thicknesses. As depicted in the figure, the relatively small variances at different thicknesses validate the reliability of the Raman lidar system for the remote sensing underwater oil.

4. CONCLUSION

This work proposes and demonstrates a single-photon Raman lidar system for underwater oil detection. In terms of hardware design, we adopted a high-performance single-photon detector to improve the detection sensitivity to the single-photon level. This allowed us to detect signals from oil at a distance of 12 m using low laser power and a small-aperture telescope, enabling the realization of a highly integrated and compact underwater lidar system. Additionally, to ensure a robust structure, the Raman lidar system employed a fiber-connected configuration. These measures laid the foundation for the effective and stable operation of the underwater Raman lidar. In terms of data processing, we established a relationship between the fitted peak amplitude and the thickness of the oil layer by fitting the backscattered signal of oil to an exponentially modified Gaussian function.

In a future work, we plan to develop another underwater Raman lidar using a laser with a shorter wavelength, such as a blue laser, to reduce the influence of chlorophyll fluorescence on the Raman backscattered signal from oil. Furthermore, to enable the operation of a single-photon Raman lidar under daylight, we will integrate it into an AUV platform. When the lidar operates underwater, the water above the lidar can act as a filter, removing a significant amount of solar radiation, especially when the lidar is operating at deeper depths. In summary, we believe that the results of this work lead to significant applications, such as remote sensing of oil leakage from underwater pipelines.

Funding. Joint Funds of the National Natural Science Foundation of China (U2106210); National Key Research and Development Program of China (2022YFB3901704); National Science Foundation of Fujian Province of China (2020J01026); MEL-RLAB Joint Fund for Marine Science & Technology Innovation.

Disclosures. The authors declare no conflicts of interest.

Data availability. The data that support the findings of this study are available from the corresponding author upon reasonable request.

REFERENCES

1. M. Ho, S. El-Borgi, D. Patil, and G. Song, "Inspection and monitoring systems subsea pipelines: a review paper," Struct. Health Monit. **19**, 606–645 (2020).
2. M. Fingas and C. Brown, "Review of oil spill remote sensing," Mar. Pollut. Bull. **83**(1), 9–23 (2014).
3. G. M. Barenboim, V. M. Borisov, V. Golosov, and A. Y. Saveca, "New problems and opportunities of oil spill monitoring systems," Proc. Int. Assoc. Hydrol. Sci. **366**, 64–74 (2015).
4. A. Shukla and H. Karki, "Application of robotics in offshore oil and gas industry—a review part ii," Robot. Auton. Syst. **75**, 508–524 (2016).
5. D. Yang, J. Guo, Q. Liu, Z. Luo, J. Yan, and R. Zheng, "Highly sensitive Raman system for dissolved gas analysis in water," Appl. Opt. **55**, 7744–7748 (2016).
6. X. Zhang, Z. Du, R. Zheng, Z. Luan, F. Qi, K. Cheng, B. Wang, W. Ye, X. Liu, and C. Lian, "Development of a new deep-sea hybrid Raman insertion probe and its application to the geochemistry of hydrothermal vent and cold seep fluids," Deep Sea Res., Part I **123**, 1–12 (2017).
7. M. Shangguan, H. Xia, C. Wang, J. Qiu, S. Lin, X. Dou, Q. Zhang, and J.-W. Pan, "Dual-frequency Doppler lidar for wind detection with a superconducting nanowire single-photon detector," Opt. Lett. **42**, 3541–3544 (2017).
8. J. H. Churnside and J. A. Shaw, "Lidar remote sensing of the aquatic environment," Appl. Opt. **59**, C92–C99 (2020).
9. A. M. Pashayev, K. R. Allahverdiyev, B. G. Tagiyev, and I. Z. Sadikhov, "Light induced fluorescence LIDAR developed and employed at the National Aviation Academy of Azerbaijan," Proc. SPIE **10226**, 102260W (2017).
10. T. A. Dolenko, V. V. Fadeev, I. V. Gerdova, S. A. Dolenko, and R. Reuter, "Fluorescence diagnostics of oil pollution in coastal marine waters by use of artificial neural networks," Appl. Opt. **41**, 5155–5166 (2002).

11. S. Harsdorf, M. Janssen, R. Reuter, S. Toeneboen, B. Wachowicz, and R. Willkomm, "Submarine lidar for seafloor inspection," Meas. Sci. Technol. **10**, 1178 (1999).
12. M. Bazzani, B. Breschi, G. Cecchi, L. Pantani, D. Tirelli, G. Valmori, P. Carlozzi, E. Pelosi, and G. Torzillo, "Phytoplankton monitoring by laser induced fluorescence," EARSeL Adv. Remote Sens. **1**, 106–110 (1992).
13. P. Pořízka, P. Prochazková, D. Prochazka, L. Sládková, J. Novotný, M. Petrilak, M. Brada, O. Samek, Z. Pilát, and P. Zemánek, "Algal biomass analysis by laser-based analytical techniques—a review," Sensors **14**, 17725–17752 (2014).
14. T. Somekawa, A. Tani, and M. Fujita, "Remote detection and identification of CO_2 dissolved in water using a Raman lidar system," Appl. Phys. Express **4**, 112401 (2011).
15. T. Somekawa, J. Izawa, M. Fujita, J. Kawanaka, and H. Kuze, "Raman lidar for remote sensing of oil in water," Appl. Opt. **60**, 7772–7774 (2021).
16. M. Shangguan, H. Xia, C. Wang, J. Qiu, G. Shentu, Q. Zhang, X. Dou, and J.-W. Pan, "All-fiber upconversion high spectral resolution wind lidar using a Fabry-Perot interferometer," Opt. Express **24**, 19322–19336 (2016).
17. C. Yu, M. Shangguan, H. Xia, J. Zhang, X. Dou, and J.-W. Pan, "Fully integrated free-running InGaAs/InP single-photon detector for accurate lidar applications," Opt. Express **25**, 14611–14620 (2017).
18. H. Xia, G. Shentu, M. Shangguan, X. Xia, X. Jia, C. Wang, J. Zhang, J. S. Pelc, M. Fejer, and Q. Zhang, "Long-range micro-pulse aerosol lidar at 1.5 μm with an upconversion single-photon detector," Opt. Lett. **40**, 1579–1582 (2015).
19. J. Xia, S. Qian, W. Wang, Z. Ning, Y. Cheng, Z. Wang, X. Li, M. Qi, Y. Heng, and S. Liu, "A performance evaluation system for photomultiplier tubes," J. Instrum. **10**, P03023 (2015).
20. X. Wang and O. C. Mullins, "Fluorescence lifetime studies of crude oils," Appl. Spectrosc. **48**, 977–984 (1994).
21. A. Ryder, T. Glynn, M. Feely, and A. Barwise, "Characterization of crude oils using fluorescence lifetime data," Spectrochim. Acta A **58**, 1025–1037 (2002).
22. J. P. Foley and J. G. Dorsey, "A review of the exponentially modified Gaussian (EMG) function: evaluation and subsequent calculation of universal data," J. Chromatogr. Sci. **22**, 40–46 (1984).